IEEE Access
Multidisciplinary | Rapid Review | Open Access Journal

SPECIAL SECTION ON THEORY, ALGORITHMS, AND APPLICATIONS OF SPARSE RECOVERY

Received January 28, 2019, accepted February 17, 2019, date of publication March 8, 2019, date of current version April 2, 2019.

Digital Object Identifier 10.1109/ACCESS.2019.2903826

Secure Remote Sensing Image Registration Based on Compressed Sensing in Cloud Setting

ZHANQIANG LIU[1], LICHENG WANG[1], XIANMIN WANG[2], XIAOYING SHEN[1], AND LIXIANG LI[1]

[1]State Key Laboratory of Networking and Switching Technology, Beijing University of Posts and Telecommunications, Beijing 100876, China
[2]School of Computer Science, Guangzhou University, Guangzhou 510006, China

Corresponding author: Xianmin Wang (xianmin@gzhu.edu.cn)

This work was supported in part by the National Key Research and Development Program of China under Grant 2016YFB0800602, in part by the National Natural Science Foundation of China (NSFC) under Grant 61502048, and in part by the Shandong Provincial Key Research and Development Program of China under Grant 2018CXGC0701.

ABSTRACT High-resolution remote sensing image registration has recently been widely applied in many fields such as agriculture, forestry, and urban planning. A high-resolution remote sensing image can depict the texture features of ground details more clearly, but it also brings new challenges to registration such as texture similarity, image storage space, and image information leakage. In this paper, to solve the above problems, we propose a finite-state chaotic compressed sensing (CS) cloud remote sensing image registration method. First, chaotic CS with a finite state not only saves storage space required for an image but also improves the security of the image in the transmission process. Next, we process the image in the cloud platform, improve the speed of image processing, and facilitate real-time data processing. Finally, we propose an improved scale invariant feature transform (SIFT) image registration method based on local and global information (LG-SIFT) that reduces the impact of texture similarity on high-resolution remote sensing images. The experimental results show that the runtime of the original processing method is twice as long as that of the proposed scheme and that the accuracy of registration improves considerably.

INDEX TERMS High-resolution remote sensing image, compressed sensing, finite-state tent chaos, global context, image registration.

I. INTRODUCTION

The first application of remote sensing image registration appeared in the military field in the 1970s. Image registration is the process of overlaying two or more images of the same scene taken at different times, from different viewpoints, and/or by different sensors [1]. Recently, it has been applied in many different fields, such as agriculture, forestry, and urban planning. For example, with respect to the Wenchuan earthquake and the Yushu earthquake, local satellite remote sensing data were acquired for the first time, which provided a reliable basis for subsequent rescue. With the improvement of remote sensing image resolution, registration of high-resolution remote sensing images creates the following new challenges. Specific performance:

- The spatial information of high-resolution remote sensing images is more abundant. Because the similarity of features between near-surface objects is more obvious, feature matching is easily disturbed by the similarity of features, which lowers the matching accuracy.
- High-resolution remote sensing images have high spatial resolution and wide width, which makes image processing difficult and storage inconvenient.
- There is a great deal of important information in high-resolution images, and information leakage easily occurs in the process of image transmission.

Currently, there are many related studies on image registration. Next, we will introduce several representative research results. In 2004, David L. proposed the scale invariant feature transform (SIFT) [2], which became a famous point matching algorithm. SIFT has good matching performance and has been widely studied for many years. In 2005, Mortensen *et al.* [3] proposed a new and improved algorithm for the similarity of local features. By extracting SIFT feature points and describing the curvature distribution of SIFT feature points in a shape context, Mortensen combined

The associate editor coordinating the review of this manuscript and approving it for publication was Jinming Wen.

them with SIFT feature descriptors to form a new descriptor. In 2010, Carmichael *et al.* [4] proposed a similar global context descriptor for speeded up robust features (SURFs) and maximally stable extremal regions (MSERs). In 2015, Kim [5] proposed a local shape context combined with SIFT descriptors, which are used for local features of a tattoo object, and a global shape is used for the overall shape of a tattoo object. Ning *et al.* [6] presented a feature matching algorithm based on a partial DAISY descriptor and global texture information. In 2017, Zhou *et al.* [7] proposed a global context verification scheme to filter false matches for copy detection. Chen *et al.* [8] proposed a novel similarity metric based on rotationally invariant regional mutual information (RIRMI). Similarity to the algorithm before, the similarity metric based on RIRMI considers not only the spatial information, but the effect of the local grey variations and rotation changes on computing probability density function as well. In this paper, an improved SIFT image registration method based on global information is proposed to reduce the texture similarity of high-resolution remote sensing images.

With the increasing resolution and data volume of remote sensing images, image processing is becoming increasingly laborious and inefficient, and the storage space required is becoming increasingly larger. At the same time, the emergence of cloud computing creates new directions for remote sensing image processing and storage. With the emergence of cloud computing, mobile operational devices and 5G high-speed networks, these emerging technologies are used in many fields, such as large-scale data computing, updating, population flow statistics, etc. [9], but they also face various security threats. Mobile cloud platform information leakage [10], [11], user privacy information theft [12], and then mainly for the transmission in the cloud and PC side. Encryption of image information in process is studied, and a method of encrypted compression synchronization based on finite state chaotic compressed sensing is proposed.

Due to their large number of pixels, remote sensing images should be compressed to reduce communication bandwidth. In addition, to protect the sensitivity of state and personal information, some encryption measures need to be adopted [13]–[17]. Compressed sensing (CS) [18], [19] is a new signal-sampling paradigm that meets a nearly optimal Nyquist sampling rate. This technology reduces the sampling points of traditional signals, such as images and videos, by utilizing in-natural redundancies. By using CS, the original picture can be reconstructed by sampling only a fraction of the data. Chaotic tent [20] systems have been widely used in image protection based on their unpredictability and sensitivity. In an image encryption algorithm based on chaotic maps, a sensing matrix is generated using chaotic sequences that uses just a symmetric key. Therefore, many scholars have conducted in-depth research on CS and chaotic cryptography.

Huang and Sakurai [21] used the characteristics of CS and proposed a compression-combined digital image encryption method. However, this type of secret key is too large to distribute and store. To solve this problem and simultaneously realize compression and encryption, Zhou *et al.* [22] proposed a new image compression-encryption hybrid method by using random measurement matrices. Liu *et al.* [23] presented a block compressed sensing (BCS) scheme by using double random phase encoding (DRPE) to enhance the security level and increase the performance of CS. This method is based on random phase encoding in the fractional Fourier domain for each image block. Based on BCS, Zhang *et al.* [24] proposed a scalable encryption framework along with the so-called Sobel edge detector and cascade chaotic maps. Therefore, based on these methods, we propose a finite-state chaotic CS method to solve the considerable storage space problem and simultaneously satisfy security. In addition, to improve the efficiency of image processing, we process images on a cloud platform.

The following contents are arranged in four sections. Section 2 presents the related methodology: CS, chaotic theory and image registration. We introduce the proposed scheme in Section 3. Next, we conduct related experiments to verify the proposed scheme in Section 4. In Section 5, we give a conclusion about the contribution of this paper.

II. THE RELATED METHODOLOGY

A. COMPRESSED SENSING

CS theory consists of three parts: sparse representation of signals, sampling of signals and reconstruction of signals.

1) SPARSE REPRESENTATION

Sparse representation of signals is the first step. Signal x is an N-dimensional vector that can be expressed by a set of linear combinatorial bases $\Psi = [\Psi_1, \Psi_2, \cdots, \Psi_M]$,

$$x = \Psi s \tag{1}$$

where Ψ is a random projection ($M < N$) dimension and s is an N-dimensional signal. If there are only K nonzero elements in the transformation coefficient $\Psi^T x$ or only K large components are retained, signal x is considered K-sparse or approximately K-sparse.

2) SAMPLING

Sampling of signals is the second step. If a vector y can be expressed as:

$$y = \Omega x \tag{2}$$

then we regard the random projection $M \times N$ dimension as the measurement matrix. y is obtained by linear projection of the signal x diagram, where y is an M-dimensional signal, and Ω is a random projection $M \times N$ dimension. FIGURE 1 shows the schematic process of signal sampling compression.

3) RECONSTRUCTION

The signal reconstruction algorithm is the third step and a key part of CS theory. The problem is how to accurately recover the original high-dimensional data from the low-dimensional data. Convex optimization indicates that the objective function of the optimization problem is a convex function, and

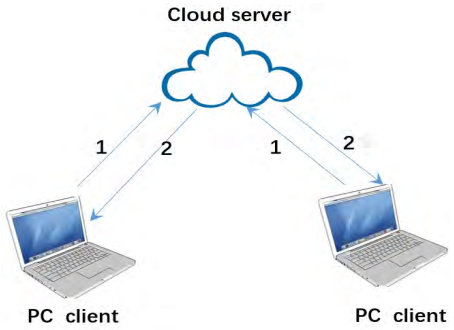

FIGURE 1. PC client upload to cloud server. PC client can upload high-resolution remote sensing images to cloud server by route 1, while PC client can download the processed images from cloud server by route 2. In this paper, we only focus on route 1.

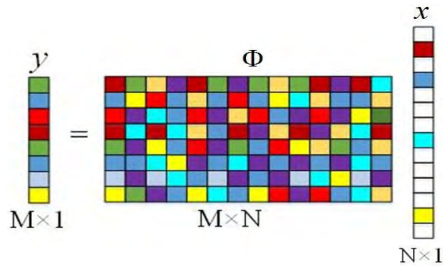

FIGURE 2. Sampling of compressed sensing.

the constrained variables are valued on the convex set. The convex optimization problem can be solved globally with sufficient computing resources, but this kind of method is often limited by the actual conditions. A nonconvex optimization algorithm has become another research direction and has high feasibility in practical applications because of its low time complexity. Many scholars have made many improvements and optimization based on OMP, for example: Wen *et al.* [25], [26] proposed two optimization algorithm. In this paper, we adopt orthogonal matching pursuit (OMP) with random measurements [27]. For OMP, random frequency measurements offer two specific advantages. The first advantage is that it can compute the maximum correlation between a signal and the columns of the matrix in time $O(d \ln d)$. The second advantage is that the matrix can be constructed and stored using only $O(N \ln d)$ bits because it is only necessary to choose N rows from a d-row matrix.

- OMP with Gaussian measurements
  Fix $\delta \in (0, 0.36)$ and choose $N \geq [K \times m \times \ln(d/\delta)]$, and draw N measurement vectors $x_1, x_2 \ldots x_N$ which are independent of the standard Gaussian distribution on R^d. Assume s is an arbitrary m-sparse signal in R^d. If the data $\{\langle s, x_n \rangle : n = 1, 2, \ldots N\}$ is given, OMP can reconstruct the signal with probability over $1 - 2\delta$. The constant satisfies $K \leq 20$.
- OMP with admissible measurements
  If we take random measurements of a sparse signal using an admissible measurement matrix, then OMP can be used to recover the original signal with high probability.
  Fix $\delta \in (0, 0.36)$, and choose $N \geq [K \times m \times \ln(d/\delta)]$. Given the data

$$v = \Gamma s \tag{3}$$

  OMP can reconstruct a signal with probability exceeding $1 - \delta$, where K is an absolute constant,s is an arbitrary m-sparse signal in R^d, and $N \times d$ is a random admissible measurement matrix Γ independent of the signal.

For Gaussian measurements, we obtained more precise estimates for the constant. Therefore, we adopt the OMP with Gaussian measurements as the reconstruction algorithm.

B. TENT CHAOTIC THEORY

Chaos is a kind of complex dynamical behavior with pseudorandom and finite special properties. The sensitivity of the initial value and the chaotic parameters are important properties in the chaotic system. This sensitivity is very suitable for encryption [28]. Moreover, the chaotic sequence is suitable for constructing the measurement matrix [29] by the deterministic method. Therefore, the measurement matrix can be used as a secret key to encrypt the plain text, which can simplify the construction process of the measurement matrix. There are many chaotic systems, such as Chebyshev, the logistic map and the tent map. Thus, we improve the method based on the tent map. The skew tent map affects the global searching capacity and computational efficiency of the chaos optimization algorithm. First, skew tent mapping [30] is a generalized tent map, which is defined as:

$$f_a(x) = \begin{cases} \dfrac{x}{a} & 0 < x \leq a \\ \dfrac{x-1}{a-1} & a < x \leq 1 \end{cases} \tag{4}$$

The structure of skew tent mapping is simple. Skew tent mapping can eliminate rounding error in the iteration process and obtain accurate numeric calculations.

C. IMAGE REGISTRATION THEORY

Currently, there are many methods based on image registration. According to the different image information used in the registration process, image registration can be divided into a region-based registration method and a feature-based registration method. In this paper, we adopt the feature point. The method based on feature points selects the corresponding feature pixels from the reference image and the image to be registered and judges them according to certain similarity criteria. If the criteria are met, the feature points are determined as feature point pairs. The similarity of the image is judged by analyzing the ratio of the correct matching points to the total matching points. The most famous method is SIFT. It is a good local image feature method. SIFT consists of four steps: scale-space extrema detection, keypoint localization, orientation assignment and keypoint descriptor.

- The first step searches over all scales and image locations. To be invariant to scale and orientation, SIFT is

implemented by adopting a difference of Gaussian function.

- The second step determines location and scale by a detailed model. Keypoints are selected based on measures of their stability.
- In the third step, one or more orientations are assigned to each keypoint location based on local image gradient directions.
- In the last step, the local image gradients are measured at the selected scale in the region around each keypoint.

III. THE PROPOSED SCHEME

In this section, we mainly elaborate on the proposed scheme, which can be roughly divided into three parts. First, we process the original image by Φ. Φ is a measurement matrix that is produced by CS and finite-state tent chaos. Therefore, CS and finite-state tent chaos can run simultaneously. Then the image can be recovered on the cloud platform by the same matrix Φ. Finally, images extracted at different times and from different angles are processed by LG-SIFT. The procedure of the proposed scheme is shown in FIGURE 3 and FIGURE 4. FIGURE 3 and FIGURE 4 are the compared schemes, we perform the experiments by these two schemes on PC and the cloud platform.

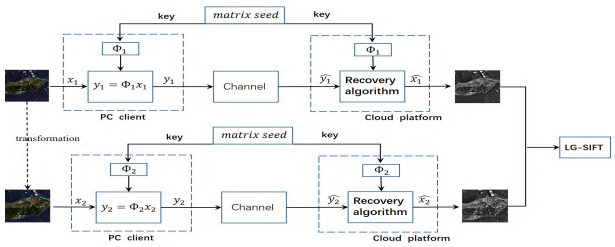

FIGURE 3. The procedure of the first compared scheme.

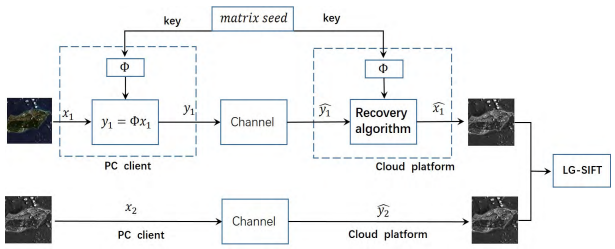

FIGURE 4. The procedure of the second compared scheme.

A. FINITE-STATE TENT CHAOTIC COMPRESSED SENSING METHOD

CS not only increases efficiency but also simultaneously encrypts the images. However, the encryption effect is not sufficient. Chaos is a kind of complex dynamical behavior with pseudorandom and finite special properties. It is suitable for encrypting plain text because of its sensitivity. In the paper "Secure and Energy-Efficient Data Transmission System Based on Chaotic Compressed Sensing in Body-to-Body Networks", Peng *et al.* [31] proposed a method to combine chaos and CS and fulfill in one step. This method simultaneously increases efficiency and encrypts the images. It also saves considerable storage space because it stores just the matrix seed rather than the whole measurement matrix. However, in the above method, the chaotic function is a two-to-one mapping, and there is no one-to-one corresponding inverse function. The inverse function is not unique and will create consistency problems during decryption so that the original cannot be restored. However, chaotic function is complex to implement. The encryption system of the skew tent mapping with finite state discretizes the skew tent mapping into one-to-one corresponding discrete mapping while retaining the chaotic characteristics of the original tent mapping. Its orbital sequence can be regarded as a Bernoulli sequence; that is, it has strong random characteristics. In this case, we propose an improved method that uses a one-to-one discretization mapping transformation finite-state method [32]. The finite state tent is defined specifically as follows: assume $M > 2$, defines the following two sets,

$$P = C = \{x; x = \frac{1}{m}, \frac{2}{m} \ldots \frac{m}{m}\} \tag{5}$$

and the transformation relation induced by the upper form is defined as follows:

$$f_a(x) = \frac{|x' \in P | f_a(x') < f_a(x)| + 1}{M} \tag{6}$$

B. LG-SIFT

The descriptors fail to consider global context and can produce ambiguity when matching, especially in texture-similar regions. In these regions, a detected feature point easily matches at least two feature points, and mismatches occur. In the introduction, there are many good methods from different angles. Most methods are based on SIFT and global context information. Moreover, by extracting the global context, the features are robust to texture-similar regions. "A SIFT Descriptor with Global Context" was the first paper to combine local information and global context. Mortensen presented a feature descriptor that augments SIFT with a global context vector. The vector adds curvilinear shape information from a larger neighborhood, and it can reduce mismatches when multiple local descriptors are similar. In this paper, we improve the method based on Mortensen's idea. We replace the shape context by relative shape context [33] and give the definition of the similarity matching measure for the relative shape context descriptor again. Compared with the shape context, the relative shape context (RSC) has many advantages, such as translation and rotation invariance. RSC is also scale invariant because it is not necessary to calculate the logarithmic distance between pairs of points. It is also robust to noise without calculating the average distance between all pairs of points in a point set when the distance term is regularized. FIGURE 5 and FIGURE 6 are the explanation of RSC.

Assuming that there are n points in point set P, the RSC of any point p_i relative to any other point p_j is $H_{p_{i,j}}(s)$. A polar

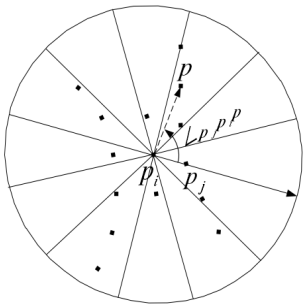

FIGURE 5. Spatial distribution of relative shape context descriptors.

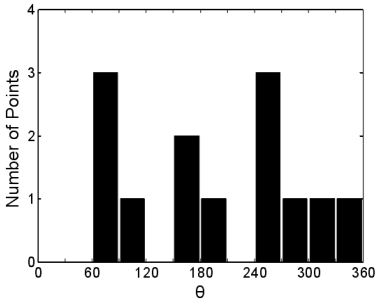

FIGURE 6. Histogram of point p_i relative to p_j relative shape context.

coordinate system is established in which, p_i is the origin and vector $\overrightarrow{p_ip_j}$ is the positive axis. $H_{p_{i,j}}(s)$ is a histogram of the polar angles of the other n-2 points in the point set relative to the positive direction of the polar coordinate system. $H_{p_{i,j}}(k)$ is:

$$H_{p_{i,j}}(k) = \sharp\{p \neq p_i, p_j \mid p, p_i, p_j \in P, \angle p_j p_i p \in bin(k)\} \quad (7)$$

where $\sharp$ is the potential of set P, $\angle p_j p_i p$ expresses anticlockwise rotation angle between vector $\overrightarrow{p_ip_j}$ and $\overrightarrow{p_ip}$. Assume point set is divided s sections, the degrees of every section is $\triangle\theta_s = \lfloor\frac{360^\circ}{s}\rfloor$. Therefore, the k-th section is:

$$bin(k) = [(k-1)\bigwedge\theta_s, k\bigwedge\theta_s] \quad (8)$$

1) LG-SIFT DESCRIPTOR

The LG-SIFT descriptor consists of two parts: a vector representing local features and a global distribution vector for removing local similarity features. We define LG-SIFT vector of this paper as follows:

$$U = \begin{bmatrix} \mu L \\ (1-\mu)G_\theta \end{bmatrix}. \quad (9)$$

where L is a 128-dimensional local description vector, G_θ is a 12-dimensional global distribution description vector, μ is the relative weight factor.

2) THE ESTABLISHMENT OF SIMILARITY MEASURES

According to the RSC, the relative shape context vector is calculated using χ^2 statistics. We construct a similarity measure as:

$$d_{G_\theta} = \chi^2 = \frac{1}{2}\sum_K \frac{(H_{p_{i,k}} - H_{p_{j,k}})^2}{H_{p_{i,k}} + H_{p_{j,k}}} \quad (10)$$

where $H_{p_{i,j}}$ is the RSC of p_i relative to p_j.

The SIFT description vector is calculated by the Euclidean distance:

$$d_L = |L_i - L_j| = \sqrt{\sum_K (L_{i,k} - L_{j,k})^2} \quad (11)$$

According to the above definition of LG-SIFT descriptor construction, the similarity measure is as follows:

$$d_{ij}(k,l) = \mu\bar{d_L} + (1-\mu)\bar{d_{G_\theta}} \quad (12)$$

where the relative weight coefficient μ is consistent with the weight coefficient in the LG-SIFT descriptor.

IV. EXPERIMENTS AND EFFECT

In this section, we perform the related experiments and then present the performance analysis based on the results of the experiments. The datasets in the experiments are from different geographical environments. Our experimental environment is an Intel(R) Core(TM) i7-6700 CPU @3.40 GHz Windows 10. The datasets run on MATLAB (version: 2015b). In the experiments, to verify the performance of the proposed method, three groups of high-resolution remote sensing images from different satellites, different phases and different widths are chosen as the test dataset. We name the datasets m1, m2, m3. Among them, m1 is from the Gaofen-2 satellite and covers the intersection of the ocean and the land at the junction. m2, which is from the WorldView-1 satellite, mainly covers the river area. m3, which is from the High-resolution 8 satellite and covers farmland. m1 and m2 are used to determine the effect of LG-SIFT. m3 is used to determine the effect of our proposed scheme.

A. EFFECT OF RECOVERY

The peak signal-to-noise ratio (PSNR) is the ratio between the maximum possible power of a signal and the power of corrupting noise that affects the fidelity of its representation. It is most commonly used to measure the quality of reconstructed images, and the higher is better in general scopes. Considering that many signals have a very wide dynamic range, PSNR (dB) is usually expressed in logarithmic decibel scale and calculated via the mean square error (MSE). That is,

$$PSNR = 10 \cdot \log_{10}(\frac{MAX^2}{MSE}) \quad (13)$$

$$MSE = \frac{1}{S \cdot R}\sum_{i=1}^{S}\sum_{j=1}^{R}[I(i,j) - K(i,j)]^2 \quad (14)$$

where S and R are the numbers of pixels of horizontal and vertical coordinates of the image, respectively, while I(i,j) and K(i,j) denote the gray matrices of the original and the reconstructed images, respectively. The constant MAX

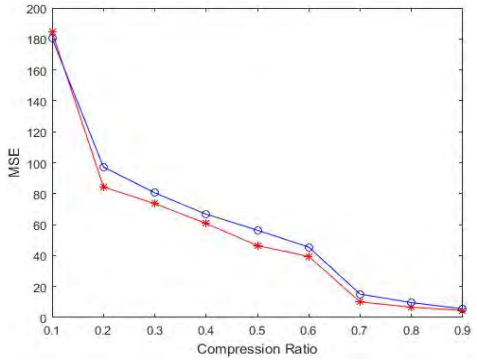

FIGURE 7. MSE at different compression ratio.

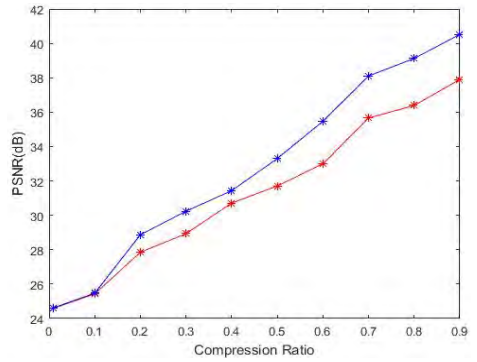

FIGURE 8. PSNR at different compression ratio.

(in this paper $2^8 - 1$) is the maximum possible pixel value of the image.

Figure 7 is the MSE of data set 2 under different compression ratios. From the above figure, we can see that when the compression ratio is between 0 and 0.2 MSE changes significantly, indicating that the image restoration is not ideal. When the compression ratio is between 0.2 and 0.6, MSE changes relatively smoothly. When the compression ratio is between 0.7 and 0.9, the change in the MSE of the image tends to be gradual, the minimum amplitude, indicating that the image restoration effect in this compression ratio interval is better.

The PSNR of two different datasets under different compression ratios is shown in Figure 7. The PSNR between the compression ratios of 0 and 0.3 is unstable. The compression ratio between 0.3 and 0.7 results in a PSNR that increases almost linearly. Compared with the range of the PSNR (approximately 20-25 dB) [34], the peak PSNR in this paper is 24 -42 dB, which shows that the proposed scheme has a great improvement in image restoration.

B. EFFECT OF RECOVERY IMAGE

From the MSE, runtime and PSNR, we can obtain a better recovery effect with a ratio of 0.7, and thus, the experiment is implemented at a compression ratio of 0.7. We will show the effect of image histogram and adjacent correlation.

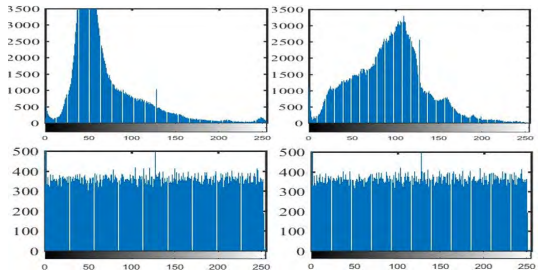

FIGURE 9. Histograms of dataset m1, m2.

1) EFFECT OF HISTOGRAM

An image histogram is a type of graphical representation of the tonal distribution in a digital image that plots the number of pixels for each tonal value. It is a very intuitive and popular tool for evaluating the encryption effectiveness for a specific image since a viewer can judge the entire tonal distribution at a glance. Through the analysis of PSNR, runtime and MSE in 4.1, we use 0.7 as the compression ratio. In this paper, m1 and m2 are selected as datasets to analyze the histograms of remote sensing images before and after encryption.

The histograms in the first row are the gray histograms of the two different datasets used in this part, showing the gray distribution of the original image pixels. It can be seen that most of the pixels in the images are less than 125, thus inferring that the gray level of the original image is dim. The images in the second row are processed by the scheme proposed in this paper. It can be seen from the images that the gray distribution is uniform and that these images are almost the same, which shows that the scheme proposed in this paper can be used as it has a better encryption effect on remote sensing images. In general, cryptographic encryption, attackers can extract the statistical features of plaintext images from ciphertext images and obtain pixels with obvious features of the original image.

2) EFFECT OF ADJACENT CORRELATION

Intuitively speaking, a good encryption scheme should map the pixel distribution of the original signal to approximately random and uniform distributions as much as possible. Therefore, adjacency correlation analysis provides us with a way to evaluate the quality of image encryption.

In our experiments, correlation analysis of adjacent pixels is shown as FIGURE 10. The first row in the figure is from the original image correlation scatter plots of different datasets, and the second row is the encrypted image pixel scatter plot distribution. From FIGURE 10, we can see that the pixels in all directions of the original image are linearly distributed, and the pixel correlation of the image is very strong. The distribution of the pixels in the encrypted images are confused and random, which indicates that the pixel distribution correlation of the image is very low, so the encryption scheme proposed in this paper is effective. We can get the same effect in FIGURE 11.

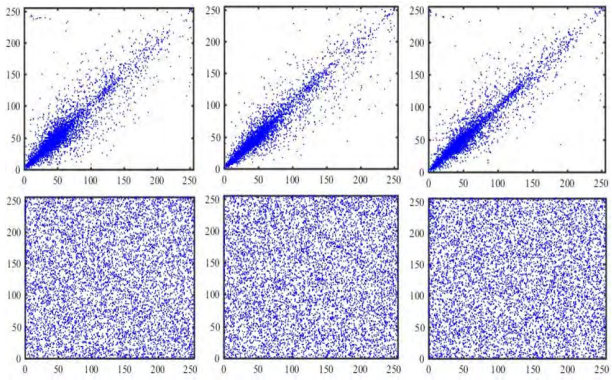

FIGURE 10. Adjacent pixel correlation analysis of dataset m1.

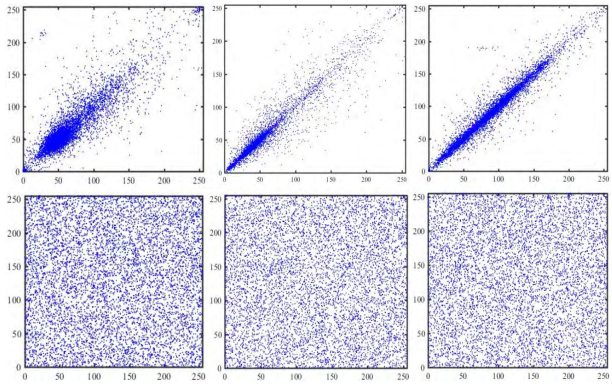

FIGURE 11. Adjacent pixel correlation analysis of dataset m2.

TABLE 1. Correlation coefficients of two datasets from different orientations.

	Horizontal		Vertical		Diagonal	
	original	processed	original	processed	original	processed
m1	0.9912	0.0031	0.9932	0.0012	0.9980	-0.0018
m2	0.9926	0.0025	0.9940	0.0023	0.9975	0.0015

We randomly select 1600 pixels from rows, columns and diagonals to calculate their respective correlation coefficients in Table 1. From the correlation coefficients of the row, column and diagonal, we can see that the correlation of the original remote sensing images is very high, and the correlation of the encrypted images tends to 0. Therefore, the encryption scheme proposed in this paper is effective for data.

C. EFFECT OF LG-SIFT

In the following, we compared the performance of SIFT, SIFT+GC, SIFT+DAISY and the proposed method (LG-SIFT) for two different high-resolution remote sensing areas. We use correct matching rates (CMR) and root MSE (RMSE) as the evaluation criteria. We evaluate the matching performance for the two experimental environments by comparing the CMR of the four methods. The registration results of different methods in the dataset are shown in Table 2, and the corresponding visual matching results are shown in FIGURE 11 and FIGURE 12.

TABLE 2. Matching results of different registration methods on the dataset m1.

Method	Correct matches	CMR	RMSE
SIFT	236	67 %	2.3
SIFT+GC	225	80 %	2.0
SIFT+DIASY	224	83 %	1.7
LG-SIFT	232	87 %	0.6

TABLE 3. Matching results of different registration methods on the dataset m2.

Method	Correct matches	CMR	RMSE
SIFT	336	72 %	2.8
SIFT+GC	317	84 %	2.0
SIFT+DIASY	314	86 %	1.8
LG-SIFT	342	89 %	0.9

From FIGURE 11, FIGURE 12, TABLE 2, and TABLE 3, the CMR of the proposed method is higher than that of the other three methods, and the RMSE is smaller. The local descriptors are poorly distinguishable due to similar textures. The SIFT+GC, SIFT+DAISY and LG-SIFT methods consider both local and global information and are robust to distinguishable texture-similar descriptors; therefore, the matching effect is better. LG-SIFT is the best method because RSC is translation invariant, rotation invariant, scale invariant and robust to noise. The experimental results show that the proposed method can obtain higher CMR and more matching pairs for remote sensing images with intensive similar textures.

D. COMPARISON OF CLOUD AND PC SERVER

Remote sensing images uploaded to the cloud can perform a series of operations, such as image fusion, location recognition, and location detection. These operations are based on accurate image registration, so the registration accuracy directly affects other subsequent processing. We process the images uploaded to the cloud. The visual effects and specific data are shown in FIGURE 14, FIGURE 15 and FIGURE 16.

FIGURE 14 is the runtime of the PC client and cloud platform on m3 under different compression ratios. From FIGURE 14, we can see that there is not much difference in running time when the compression ratio is smaller than 0.5. When the compression ratio is larger than 0.5, the PC runtime is longer than that of the cloud platform.

FIGURE 15 is a countryside area that contains many crops. In this figure, the pair of the second line is the image deformation of the first line. We compare these two pairs to check what influence the proposed method would be as FIGURE 3. Feature points are prone to mismatches because crops are similar in appearance. Line 1 and Line 2 were processed by the same method(finite-state tent chaotic CS). Then, we process the images by LG-SIFT. From FIGURE 15, the influence of pixel features on the image can be neglected, which shows the reliability of the proposed scheme.

FIGURE 16 is another experiment. In this experiment, we match the original image and the deformed image to check

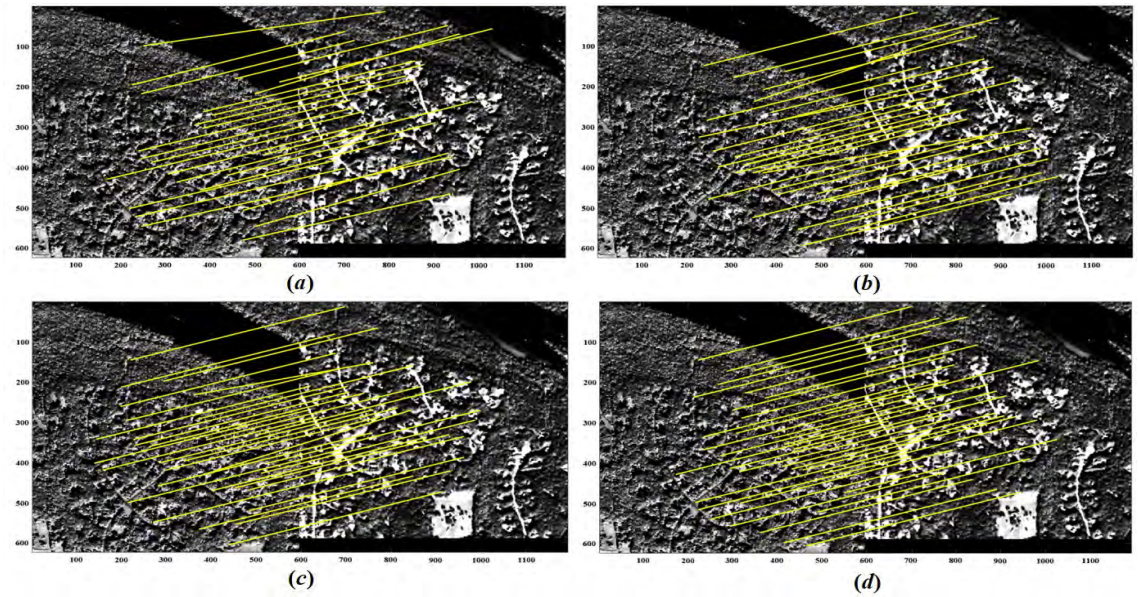

FIGURE 12. Visual effects of remote sensing image registration of dataset m1.

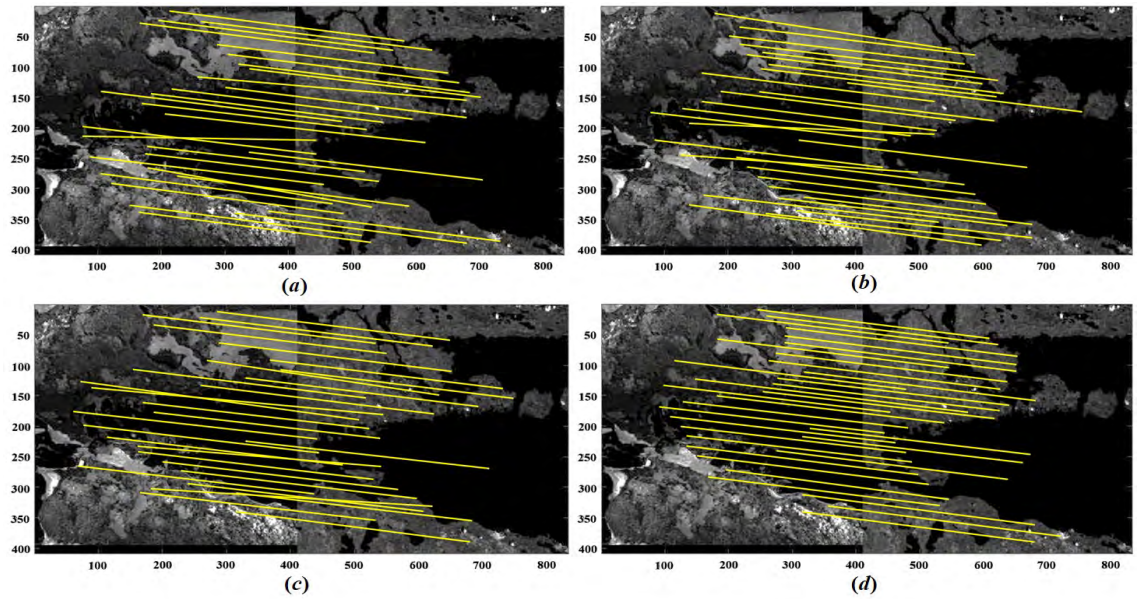

FIGURE 13. Visual effects of remote sensing image registration of dataset m2.

what influence would be using the same image as FIGURE 4. In the first line, we process the original image by finite-state tent chaotic CS. We do not any process on Line 1, just send it to the cloud platform. Then, we process these two images by LG-SIFT. From FIGURE 16, the influence of pixel features on the image can be neglected, which shows the reliability of the proposed scheme.

Table 3 and Table 4 are the digital representation of the countryside area images, which can more intuitively illustrate the loss degree of the proposed scheme to the image features. I1 and I2 are different images in the same scene. For I1, the number of match pairs is 1720, the number of correct

TABLE 4. Correct ratio of original image and processed image on dataset m3.

	match pairs	correct pairs	correct ratio
I1	2250	2137	95 %
I2	1986	1827	92 %

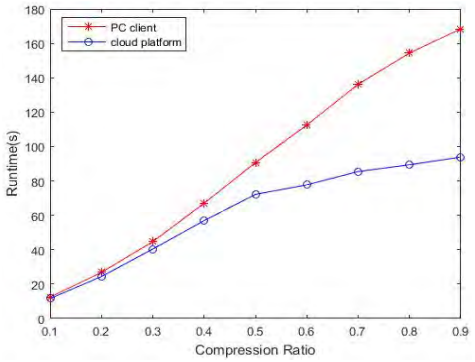

FIGURE 14. Running time at different compression ratio.

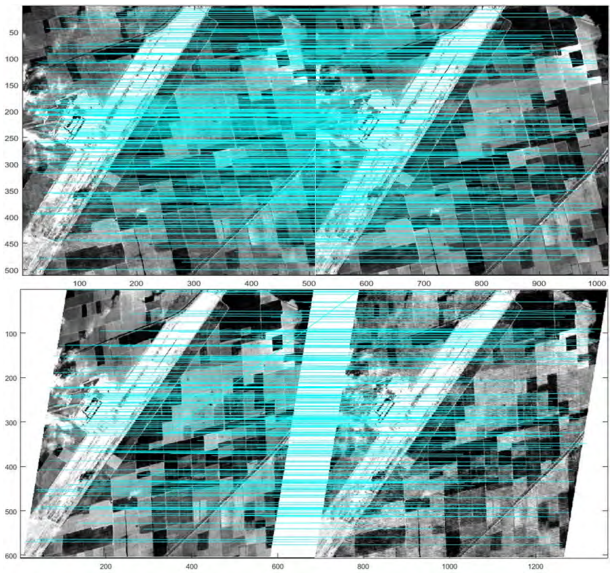

FIGURE 15. Visual effects of dataset m3.1 image registration. Line 1 and line 2 are the different images, which are processed by the proposed method. Images in line 2 are the transformed by line 1.

TABLE 5. Correct ratio of original image and processed image on dataset m3.

	match pairs	correct pairs	correct ratio
I3	1720	1532	89 %
I4	1318	1144	87 %

pairs is 1532, the correct matching rate is 89.07%. For I2, the number of total pairs is 1318, the number of correct pairs is 1144, the correct matching rate is 86.82%. I3 and I4 are different lines in the FIGURE 16. For I3, the number of match pairs is 1720, the number of correct pairs is 1532, and the correct matching rate is 89.07%. For I4, the number of total pairs is 1318, the number of correct pairs is 1144, and the correct matching rate is 86.82%. The numerical results show that the proposed compressed and chaotic scheme has approximately 2% loss on the different images, and most of the image features are retained. Therefore, the effects are

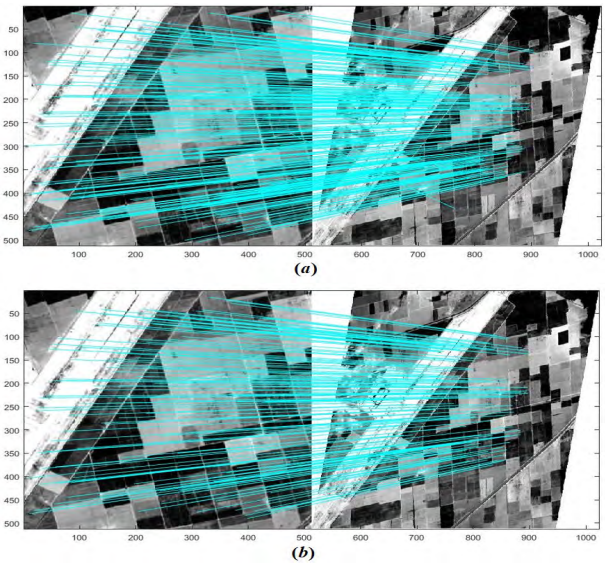

FIGURE 16. Visual effects of dataset m3.2 image registration. In the first line, the first image is original image and the second image is the deformation image on cloud platform. In the second line, the order of images is the same as the first line, but the images in Line 1 is not processed by chaos and CS.

good unless we have a high accuracy demand on original images and processed images.

V. CONCLUSION

Remote sensing image registration has been widely used in many fields in recent years. However, with the improvement of the resolution, it also brings new challenges to registration, such as texture similarity, image storage space, and image information leakage. In this paper, to solve the above problems, we propose a finite-state chaotic CS cloud remote sensing image registration method. First, chaotic CS with a finite state not only saves image storage space but also improves the security of the image in the transmission process. Then, we process the image in the cloud platform to improve the speed of image processing, and facilitate real-time data processing. Finally, we propose an improved remote sensing image registration method based on local and global information that reduces the impact of texture similarity on high-resolution remote sensing images. The simulation results show that the performance of the proposed scheme is excellent for runtime and encryption and for matching accuracy rates.

REFERENCES

[1] S. Dawn, V. Saxena, and B. Sharma, "Remote sensing image registration techniques: A survey," in *Proc. Int. Conf. Image Signal Process.* Berlin, Germany: Springer, 2010, pp. 103–112.
[2] D. G. Lowe, "Distinctive image features from scale-invariant keypoints," *Int. J. Comput. Vis.*, vol. 60, no. 2, pp. 91–110, Nov. 2004.
[3] E. N. Mortensen, H. Deng, and L. G. Shapiro, "A SIFT descriptor with global context," in *Proc. IEEE Comput. Soc. Conf. Comput. Vis. Pattern Recognit. (CVPR)*, vol. 1, Jun. 2005, pp. 184–190.

[4] G. Carmichael, R. Laganiére, and P. Bose, "Global context descriptors for surf and MSER feature descriptors," in *Proc. Can. Conf. Comput. Robot Vis.*, May/Jun. 2010, pp. 309–316.
[5] J. Kim, A. Parra, J. Yue, H. Li, and E. J. Delp, "Robust local and global shape context for tattoo image matching," in *Proc. IEEE Int. Conf. Image Process. (ICIP)*, Sep. 2015, pp. 2194–2198.
[6] G. Ning, "A SIFT matching algorithm based on global context DAISY descriptor," *Sci. Surveying Mapping*, 2016.
[7] Z. Zhou, Y. Wang, Q. M. J. Wu, C. Yang, and X. Sun, "Effective and efficient global context verification for image copy detection,"*IEEE Trans. Inf. Forensics Security*, vol. 12, no. 1, pp. 48–63, Jan. 2017.
[8] S. Chen, X. Li, L. Zhao, and H. Yang, "Medium-low resolution multisource remote sensing image registration based on SIFT and robust regional mutual information," *Int. J. Remote Sens.*, vol. 39, no. 10, pp. 3215–3242, Jan. 2018.
[9] H. Li, H. Zhu, and D. Ma, "Demographic information inference through meta-data analysis of Wi-Fi traffic," *IEEE Trans. Mobile Comput.*, vol. 17, no. 5, pp. 1033–1047, May 2018.
[10] L. Wei *et al.*, "Security and privacy for storage and computation in cloud computing," *Inf. Sci.*, vol. 258, pp. 371–386, Feb. 2014.
[11] M. Li, N. Ruan, Q. Qian, H. Zhu, X. Liang, and L. Yu, "SPFM: Scalable and privacy-preserving friend matching in mobile cloud," *IEEE Internet Things J.*, vol. 4, no. 2, pp. 583–591, Apr. 2017.
[12] H. Li *et al.*, "Privacy leakage of location sharing in mobile social networks: Attacks and defense," *IEEE Trans. Dependable Secure Comput.*, vol. 15, no. 4, pp. 646–660, Jul./Aug. 2018.
[13] X. Chen, J. Li, J. Weng, J. Ma, and W. Lou, "Verifiable computation over large database with incremental updates," *IEEE Trans. Comput.*, vol. 65, no. 10, pp. 3184–3195, Oct. 2015.
[14] X. Chen, J. Li, X. Huang, J. Ma, and W. Lou, "New Publicly Verifiable Databases with Efficient Updates," *IEEE Trans. Dependable Secure Comput.*, vol. 12, no. 5, pp. 546–556, Sep./Oct. 2015.
[15] X. Chen, J. Li, J. Ma, Q. Tang, and W. Lou, "New algorithms for secure outsourcing of modular exponentiations," *IEEE Trans. Parallel Distrib. Syst.*, vol. 25, no. 9, pp. 2386–2396, Sep. 2014.
[16] H. Yuan, X. Chen, T. Jiang, X. Zhang, Z. Yan, and Y. Xiang, "DedupDUM: Secure and scalable data deduplication with dynamic user management," *Inf. Sci.*, vol. 456, pp. 159–173, Aug. 2018.
[17] X. Zhang, T. Jiang, K.-C. Li, A. Castiglione, X. Chen, "New publicly verifiable computation for batch matrix multiplication," *Inf. Sci.*, vol. 479, , pp. 664–678, Apr. 2017.
[18] E. J. Candes and T. Tao, "Near-optimal signal recovery from random projections: Universal encoding strategies," *IEEE Trans. Inf. Theory*, vol. 52, no. 12, pp. 5406–5425, Dec. 2006.
[19] D. L. Donoho, "Compressed sensing," *IEEE Trans. Inf. Theory*, vol. 52, no. 4, pp. 1289–1306, Apr. 2006.
[20] C. Li, G. Luo, Q. Ke, and C. Li, "An image encryption scheme based on chaotic tent map," *Nonlinear Dyn.*, vol. 87, no. 1, pp. 127–133, 2017.
[21] R. Huang and K. Sakurai, "A robust and compression-combined digital image encryption method based on compressive sensing," in *Proc. 7th Int. Conf. on Intell. Inf. Hiding and Multimedia Signal Process., (IIH-MSP)*, Dalian, China, Oct. 2011, pp. 105–108.
[22] N. Zhou, A. Zhang, F. Zheng, and L. Gong, "Novel image compression–encryption hybrid algorithm based on key-controlled measurement matrix in compressive sensing," *Opt. Laser Technol.*, vol. 62, pp. 152–160, Oct. 2014.
[23] H. Liu, Y. B. Liu, and G. X. Xu, "Securely compressive sensing using double random phase encoding," *Adv. Mater. Res.*, vol. 20, no. 5, pp. 926–930, 2014.
[24] Y. Zhang *et al.*, "A block compressive sensing based scalable encryption framework for protecting significant image regions," *Int. J. Bifurcation Chaos*, vol. 26, no. 11, pp. 1–15, 2016.
[25] N. Zhou, A. Zhang, J. Wu, D. Pei, and Y. Yang, "Novel hybrid image compression–encryption algorithm based on compressive sensing," *Optik*, vol. 125, no. 18, pp. 5075–5080, 2014.
[26] J. Wen, H. Chen, and Z. Zhou, "An optimal condition for the block orthogonal matching pursuit algorithm," *IEEE Access*, vol. 6, pp. 38179–38185, 2018.
[27] J. Wen, Z. Zhou, J. Wang, X. Tang, and Q. Mo, "A sharp condition for exact support recovery with orthogonal matching pursuit," *IEEE Trans. Signal Process.*, vol. 65, no. 6, pp. 1370–1382, Mar. 2017.
[28] J. A. Tropp and A. C. Gilbert, "Signal recovery from random measurements via orthogonal matching pursuit," *IEEE Trans. Inf. Theory*, vol. 53, no. 12, pp. 4655–4666, Dec. 2007.
[29] M. Frunzete, L. Yu, J.-P. Barbot, and A. Vlad, "Compressive sensing matrix designed by tent map, for secure data transmission," in *Proc. Signal Process. Algorithms, Architectures, Arrangements, Appl. SPA*, 2011, pp. 1–6.
[30] L. Yu, J. P. Barbot, G. Zheng, and H. Sun, "Compressive sensing with chaotic sequence," *IEEE Signal Process. Lett.*, vol. 17, no. 8, pp. 731–734, Aug. 2010.
[31] H. Peng, Y. Tian, J. Kurths, L. Li, Y. Yang, and D. Wang, "Secure and energy-efficient data transmission system based on chaotic compressive sensing in body-to-body networks," *IEEE Trans. Biomed. Circuits Syst.*, vol. 11, no. 3, pp. 558–573, Jun. 2017.
[32] P. Tino and M. Koteles, "Extracting finite-state representations from recurrent neural networks trained on chaotic symbolic sequences," *IEEE Trans. Neural Netw.*, vol. 10, no. 2, p. 284, Mar. 1999.
[33] J. Zhao, S. L. Zhou, J. X. Sun, and Z. Li, "Point pattern matching using relative shape context and relaxation labeling," in *Proc. 2nd IEEE Int. Conf. Adv. Comput. Control (ICACC)*, Shenyang, China, Mar. 2010, pp. 516–520.
[34] N. Thomos, N. V. Boulgouris, and M. G. Strintzis, "Optimized transmission of JPEG2000 streams over wireless channels," *IEEE Trans. Image Process.*, vol. 15, no. 1, pp. 54–67, Jan. 2005.

ZHANQIANG LIU received the B.S. degree from the University of Jinan, in 2016. He is currently pursuing the M.S. degree with the Beijing University of Posts and Telecommunications. His current research interests include network security, remote sensing, image registration.

LICHENG WANG received the Ph.D. degree from Shanghai Jiao Tong University, in 2007. He is currently an Associate Professor with the Beijing University of Posts and Telecommunications, Beijing, China. His current research interests include modern cryptography, network security, and trust management.

XIANMIN WANG received the B.S. degree from Suzhou University, Jiangsu, China, in 2006, the M.S. degree in computer science from the Jiangxi University of Science and Technology, Jiangxi, China, in 2013, and the Ph.D. degree in computer science from Beihang University, in 2017. He is currently with the School of Computer Science, Guangzhou University. His research interests include deep learning, and image processing and understanding.

XIAOYING SHEN received the M.S. degree from Northwest Normal University, in 2017. She is currently pursuing the Ph.D. degree with the Beijing University of Posts and Telecommunications. Her current research interests include network security, blockchain technology, and isogeny-based cryptography.

LIXIANG LI received the M.S. degree in circuit and system from Yanshan University, Qinhuangdao, China, in 2003, and the Ph.D. degree in signal and information processing from the Beijing University of Posts and Telecommunications, Beijing, China, in 2006. She has co-authored over 100 papers. She was a visiting professor with the Institute for Climate Impact Research, Potsdam, Germany, in 2011. She is currently a Professor with the School of Cyberspace Security, Beijing University of Posts and Telecommunications. Her research interests include compressive sensing, swarm intelligence, and network security. She was a recipient of the National Excellent Doctoral Theses Winner, the New Century Excellent Talents in University, Hong Kong Scholar Award Winner, and Beijing Higher Education Program for Young Talents Winner.